ISSN 0915-633X

NATIONAL INSTITUTE FOR FUSION SCIENCE

Orbital Aspects of Reachable β Value in NBI Heated Heliotron/Torsatrons

S. Murakami, N. Nakajima, S. Okamura and M. Okamoto

(Received - May 9, 1995)

NIFS-354 May 1995

RESEARCH REPORT
NIFS Series

NAGOYA, JAPAN

Orbital Aspects of Reachable β Value in NBI heated Heliotron/Torsatrons

S. Murakami, N. Nakajima, S. Okamura and M. Okamoto
National Institute for Fusion Science,
Nagoya 464-01, Japan

Abstract

By modeling the typical orbital deviation and the deposition profile of tangentially injected neutral beams, the heating efficiency is derived in heliotron/torsatrons. It is found that the changes of the configuration due to the finite β effects alter the NBI heating efficiency largely and that the magnetic well or hill condition, which is important for the MHD stabilities, is also an important factor to determine the heating efficiency in a weak magnetic field. By combining the energy confinement scaling law the reachable β value is evaluated and it is found that there is the optimum value of the magnetic field strength to obtain the high plasma β in a point of view of the NBI heating efficiency.

Keywords: plasma beta, heliotron / torsatron, neutarl beam injection heating, beam orbit loss, heating effiiency, high beta experiments, the Compact Helical System

Physics of high β (=the kinetic pressure/the magnetic pressure) plasma is one of the important issues for developing the efficient future fusion reactor and many experimental and theoretical studies have been done not only in tokamaks[1,2] but also in heliotron/torsatrons[3-8]. Especially in heliotron/torsatrons the possibility of operations with currentless high β plasma is a good advantage and it is necessary to understand the physics in the high β plasma. Recently the high β experiments in the CHS (Compact Helical System)[9] show the highest averaged beta value in heliotron/torsatrons as $\beta = 2.1\%$[7,8].

Since the CHS is the low aspect ratio device the stability limit is sufficiently high due to the magnetic well created by the Shafranov shift and it is considered that the plasma β would be limited by the equilibrium limit. However the obtained maximum β value of CHS experiments is lower than the expected value by the equilibrium limit. Additionally there is a clear magnetic field strength dependence that the maximum β value is obtained with $B_0 \sim 0.6$T and that the β value is sharply decreased with $B_0 \sim 0.5$T. These facts show that there exists other mechanism to limit the plasma β depending on the magnetic field strength and configuration in heliotron/torsatrons.

The averaged plasma beta, β, is estimated in terms of the heating power of the tangentially injected NBI, P_h, and the energy confinement time, τ_E, by

$$\beta = \frac{2}{3} \frac{P_h \tau_E}{\int \frac{1}{2\mu_0} B^2 \mathrm{d}V}, \qquad (1)$$

where B and μ_0 are the magnetic field strength and the vacuum magnetic permeability, respectively. Even if the field dependence of τ_E is taken into consideration as $\tau_E \propto B^\gamma$ ($\gamma = 0.7 \sim 0.9$), a very high β plasma is obtained in a very weak magnetic field when the magnetic field dependence of P_h is ignored. Actually, however, the efficiency of NBI heating decreases to reduce the β value when the strength of magnetic field becomes too small[8]. This fact clearly indicates that the deviation of the drift orbits of the tangentially injected NBI particles is large in the weak magnetic field as well as perpendicular injection in heliotron/torsatrons with a low aspect ratio. In this paper, by modeling the typical orbital deviation and the birth deposition profile of tangentially injected beam particles the orbital aspects of the heating efficiency and the reachable β value are examined in heliotron/torsatrons.

The drift motions of injected beam particles mainly consist of two kinds of motions across the magnetic surface in heliotron/torsatrons. One is the drift motion due to the axisymmetric magnetic field components, $\langle B \rangle$, which causes the shift of the drift surface from the magnetic surface. The other is the motion due to the helical magnetic field components, B_h, which causes the small circulation motions around the drift orbit given by the axisymmetric components. Figure 1 shows a schematic view of these two types of drift motions in magnetic flux coordinates for the co injection beam particle, where the shift of the drift surface is outward. Estimating these two drift motions, which are typically expressed by Δ_d and Δ_h in Fig. 1, we can evaluate the prompt orbit loss of tangentially injected beam particles leading to the reduction of the NBI heating efficiency.

When the drift motions due to $\langle B \rangle$ are assumed to draw the co-centric circles on the poloidal cross section in the magnetic flux coordinates as shown in Fig. 1 those motions are predicted only by calculating the center position of the drift circles. Since the equations of motion are given by simple forms in the Boozer coordinates we here evaluate values Δ_d and Δ_h in the Boozer coordinates (ψ, θ, ϕ). At the center of the drift surface the particle dose not move in the poloidal direction , $\langle \dot{\theta} \rangle = 0$ at $\theta = 0$ (co injection) and $\theta = \pi$ (counter injection), where $\langle \rangle$ indicates the average over one helical pitch. Thus, from the equations of motion in the Boozer coordinates[10] the condition for the drift center is given by

$$\left\langle \left(\delta \frac{\partial B}{\partial \psi} + q \frac{\partial \Phi}{\partial \psi} \right) \frac{g}{\gamma} - \frac{q^2 B^2 \rho_{\parallel}}{M_b} \frac{(\rho_{\parallel} g' - \iota)}{\gamma} \right\rangle = 0, \tag{2}$$

(the meaning of the notation is mentioned in Ref. 10).

For the tangentially injected particles the parallel velocity $v_{\parallel}$ is much larger than $v_{\perp}$ and $\delta \sim q^2 \rho_{\parallel}^2 B / M_b$. By assuming the small effects of radial electric field, $\left| \delta \frac{\partial B}{\partial \psi} \right| \gg q \left| \frac{\partial \Phi}{\partial \psi} \right|$, and no net toroidal current, $I = 0$, the condition for the drift center is expressed as

$$\sigma B_0 g(\psi_c) \rho_{\parallel 0} \frac{d}{d\psi} \langle B(\psi_c, \theta_b) \rangle - \sigma \rho_{\parallel 0} g'(\psi_c) B_0 \langle B(\psi_c, \theta_b) \rangle + \iota \left(\langle B(\psi_c, \theta_b) \rangle \right)^2 = 0. \tag{3}$$

where $\theta_b = 0$ and $\sigma = 1$ for co injection case, and $\theta_b = \pi$ and $\sigma = -1$ for counter injection case. $\rho_{\parallel 0}$ and ψ_c are the parallel gyroradius ($= \sqrt{2 M_b E_b} / q B_0$) and the drift center position in the ψ coordinate, respectively. Since the averaged minor radius r is given by $r = \sqrt{2\psi / B_0}$, the shift of the drift surface from the magnetic axis, Δ_d, is expressed in terms of ψ_c by $\Delta_d = \sigma \sqrt{2\psi_c / B_0}$.

For the simple case with constant $\iota(\psi)$, ι_0, and $\langle B(\psi,\theta)\rangle = B_0\{1 - \epsilon_t\sqrt{\psi/\psi_a}\cos\theta + \epsilon_0\psi/\psi_a\}$, the shift of the drift surface is given by

$$\Delta_d = \sigma\frac{\rho_{\|0}}{\iota_0}\frac{1}{1+\sigma 2\frac{\epsilon_0}{\epsilon_t}\frac{\rho_{\|0}}{a\iota_0}} \tag{4}$$

where we assume $\epsilon_t \sim |\epsilon_0| \sim (B_0 a/g_0) \ll 1$. It is found that the shift of the drift surface is primary determined by the toroidicity, ϵ_t, and that the magnetic well ($\epsilon_0 > 0$) or hill ($\epsilon_0 < 0$) configuration modifies that value. In the configuration with the magnetic well ($\epsilon_0 > 0$), the shift is reduced in the co injection case ($\sigma = 1$) and is enhanced in the counter injection case ($\sigma = 0$).

The drift motion due to B_h would expressed as a circulation motion around the drift surface due to $\langle B\rangle$. To estimate the excursion due to such a drift motion, it is assumed that the helical component of the magnetic field is written as $B_h = \sum_m B_{m,N}\cos(m\theta - N\phi)$. The radial motion due to these modes, $\{\dot\psi\}_h$, is given by[10]

$$\begin{aligned}\{\dot\psi\}_h &= \rho_{\|0}^2\omega_c\sum_m mB_{m,N}\sin(m\theta - N\phi), && (5)\\ &\simeq \rho_{\|0}^2\omega_c\sum_m mB_{m,N}\sin(-\omega(m)t + \phi_0), && (6)\end{aligned}$$

where $\omega(m) \simeq \sigma(N - \iota m)\left|v_\|\right|/R$. Then the radial excursion is written as

$$\Delta\{\psi\}_h = -\rho_{\|0}^2\omega_c\sum_m \frac{mB_{m,N}}{\omega(m)}\cos(m\theta - N\phi) \tag{7}$$

and the radial excursion due to the helical component B_h, Δ_h, is given by

$$\Delta_h = \sqrt{r_d^2 + \frac{2}{B_0}\Delta\{\psi\}_h} - r_d, \tag{8}$$

where r_d is the radial position given by the motion due to axisymmetric component $\langle B\rangle$. In the followings the value of Δ_h is evaluated at $\theta = 0$ ($\theta = \pi$) for co (counter) injection case where ϕ is determined to get the largest excursion of orbits. By neglecting the effects of the reentering particles, the last closed magnetic surface is used as the loss boundary. Thus particles passing through the radial point r, $r > a$, are thought to be lost.

In order to estimate the heating efficiency the profile of the beam deposition should be given. Based on the beam depositions obtained by the Monte Carlo simulation analyses we found out that the birth deposition profile is given by the following simple form:

$$n_b = n_0 \left\{ 1 - \frac{(x-\delta_N)^2 + y^2}{(a-\delta_N)^2} \right\}, \tag{9}$$

where δ_N is the shift of the peak position of the birth deposition profile, which depends on the density, the injected beam energy, and the configuration of the equilibrium. The coordinates x and y are shown in Fig. 1. The total deposition number N_{b0} and the heating efficiency η are given by $N_{b0} = \frac{\pi}{2} n_0 (a-\delta_N)^2$ and $\eta = \frac{1}{N_{b0}} \int_S n_b \, dxdy$, respectively, where the region S is shown in Fig. 2 for three cases; a) the co injection case with $2\delta_N - 2\Delta_d - \Delta_h \geq 0$, b) the co injection case $2\delta_N - 2\Delta_d - \Delta_h < 0$, and c) the counter injection case. The shaded regions show the beam deposit regions and dotted circles indicate the most outer confined drift orbit given by Δ_d (the least distance between the dotted circles and the last closed magnetic surface is Δ_h). Finally the heating efficiency is obtained as

$$\begin{aligned}
\eta &= \frac{P_h}{P_0} \\
&= \frac{\rho_d^2}{2\rho_N^4}(2\rho_N^2 - \rho_d^2 - 2\Delta_N^2) + \frac{2}{3\pi}\frac{(4\Delta_N - x_d)}{\rho_N^4}(\rho_d^2 - x_d^2)^{3/2} \\
&\quad - \frac{1}{\pi}\frac{(2\rho_N^2 - \rho_d^2 - 2\Delta_N^2)}{\rho_N^4}\left\{ x_d\sqrt{\rho_d^2 - x_d^2} + \rho_d^2 \arcsin\frac{x_d}{\rho_d} \right\} + \frac{x_N}{\pi\rho_N^2}\sqrt{\rho_N^2 - x_N^2} \\
&\quad + \frac{1}{\pi}\arcsin\frac{x_N}{\rho_N} + \frac{2}{3\pi}\frac{x_N}{\rho_N^4}(\rho_N^2 - x_N^2)^{3/2} + \frac{1}{2},
\end{aligned} \tag{10}$$

where

$$\begin{aligned}
&\rho_N = a - \delta_N, && x_N = x_c - \delta_N, \\
&\rho_d = a - \sigma(\Delta_d + \Delta_h), && x_d = x_c - \Delta_d, \\
&\Delta_N = \delta_N - \Delta_d, && x_c = \frac{2a\{\delta_N - \sigma(\Delta_d - \Delta_h)\} + 2\Delta_d\Delta_h + \Delta_h^2}{2(\delta_N - \sigma\Delta_d)}.
\end{aligned} \tag{11}$$

For case b) (co injection with $2\delta_N - 2\Delta_d - \Delta_h < 0$), $x_d = -\rho_d$ and $x_N = -\rho_N$ hold, and for counter injection with $\Delta_h \leq \delta_N$, which is not shown in Fig. 2 $x_d = -\rho_d$ and $x_N = -\rho_N$ also hold. For the very simple co injection case where $\Delta_d = \rho_{\|0}/\iota_0$, $\delta_N = 0$, $\Delta_h = 0$ (case b)), the heating efficiency is given from Eq. (10) as

$$\eta = \left(1 - \frac{\rho_{\|0}}{\iota_0 a}\right)^3 \left(1 + 3\frac{\rho_{\|0}}{\iota_0 a}\right). \tag{12}$$

By assuming the energy confinement time as $\tau_E = F(n, a, R)B^\gamma P_h^{-\alpha}$, $(2 > \gamma > 0$ and

$1 > \alpha > 0$), and substituting both τ_E and Eq. (12) into Eq. (1), the β is expressed as

$$\beta = F' P_0^{1-\alpha} B^{\gamma-2} \left\{ \left(1 - \frac{\rho_{\parallel 0}}{\iota_0 a}\right)^3 \left(1 + 3\frac{\rho_{\parallel 0}}{\iota_0 a}\right) \right\}^{1-\alpha} . \quad (13)$$

The maximum value of β is obtained as

$$\beta_{max} = F' \left\{ \left(1 - \frac{1}{k}\right)^3 \left(1 + \frac{3}{k}\right) \right\}^{1-\alpha} \left(\frac{M_b v_b}{q \iota_0 a}\right)^{\gamma-2} P_0^{1-\alpha} \text{ at } B = \frac{k M_b v_b}{q \iota_0 a}, \quad (14)$$

where v_b is the beam velocity and $k = \sqrt{1 + 3(6 - 4\alpha - \gamma)/(2 - \gamma)} - 1$. Eq. (14) shows the existence of optimum magnetic field strength for high β operation in a point of view of orbital effects through heating efficiency. It is found that the optimum magnetic field strength is proportional to the beam velocity and $1/\iota_0$ and higher β_{max} is obtained with lower beam velocity and higher rotational transform.

Here our model is applied to the CHS plasma and compared with the results of high β experiments. The total power of NBI heating in the CHS is 1.8MW (the co injection power $P_{co0} = 1.1$MW and the counter injection power $P_{cnt0} = 0.7$MW) and beam energies are 40keV for co injection and 36keV for counter injection, respectively. Here we only consider the primary beam energy component and effects of multi energy components are not considered. The averaged plasma density is assumed to $\langle n \rangle = 0.55 \times 10^{20}\mathrm{m}^{-3}$ in this calculation. We use the magnetic field components and ι obtained by the three dimensional MHD equilibrium using the VMEC code with the pressure profile $p = p_0(1 - \psi/\psi_a)^2$. The large change of the the magnetic field components and ι can be observed due to finite β effects, i. e., a large Shafranov shift[8]. Applying these values to Eqs. (4), (8), and (10) we can obtain the heating efficiency in the CHS.

Figures 3-(A) and (B) show the heating efficiency η as a function of the magnetic field strength B for configurations with different β, where we use the δ_N obtained by the beam deposition code[11]. Since the δ_N is large for the used high density plasma, the heating efficiency in the co injection case is higher than that in the counter injection case (As is understood from Fig. 2.). As β increases, the large Shafranov shift makes the configuration with magnetic well. Thus the shift of the drift center, Δ_d, is reduced for co injected beam and enlarged for counter injected beam. We can see the increasing (decreasing) of the heating efficiency with β at the weak magnetic region for co (counter) injection case. Also the deviation Δ_h due to the helical component B_h is enlarged in the configuration with higher β and the losses of particles are enhanced by the motion due to the helical component. The reductions of the heating efficiency due to this effect can be seen clearly at the region $B > 0.8$T for the configurations with β = 1.83% and 2.38% in the co injection case (Fig. 3-(A)). Since the Shafranov shift modifies the density profile along the beam line largely, δ_N depends on β as well as the density. δ_N is reduced as β increases, which is the reason why the heating efficiency increases with β for the counter injection at $B > 1$T in Fig. 3-(B).

Combining the energy confinement time τ_E to the heating efficiency η we can evaluate β by Eq. (1). In heliotron/torsatrons the LHD scaling is used for expressing the energy confinement time. The LHD scaling for the energy confinement time, τ_E^{LHD}, is given by[12]

$$\tau_E^{LHD} = 0.17 R^{0.75} a^2 n^{0.69} B^{0.84} P_h^{-0.58}, \tag{15}$$

where R, a, n, B, and P_h are the major radius [m], minor radius [m], density [10^{20}m^{-3}], magnetic field strength [T], and injected power [MW]. Substituting Eq. (15) to Eq. (1) β is written as

$$\beta = 0.0144 R^{-0.25} n^{0.69} B^{-1.16} P_h^{0.42}, \tag{16}$$

where we assume $\int \frac{B^2}{2\mu_0} \mathrm{d}V = \pi^2 a^2 R B_0^2/\mu_0$. The plots of β as a function of the magnetic field strength for configurations with different β corresponding to the CHS experiment are shown in Fig. 4.

In the stronger magnetic field region ($B > 1.0$T) the obtained β is roughly independent of configurations, because the heating efficiencies of co injection are nearly unity and constant in this region. On the other hand, the contribution of counter injection is small because of the lower heating efficiency and smaller heating power than those of co injection. In the weaker magnetic field region ($B < 1.0$T) the heating efficiency depends strongly on B and configurations, leading to the different β_{max}. In the vacuum configuration case β_{max} is obtained at $B \sim 0.9$T and the obtainable β value becomes 0 at $B \sim 0.45$T. The β_{max} is increased until the configuration with β = 1.83% but is decreased in the configuration with β = 2.38% because of the large amplitude of Δ_h which leads to the decreasing of the heating efficiency.

In order to compare the reachable β with experimental β we calculate β using the configuration consistent with the obtained β. Figure 5 shows the plot of reachable β in terms of the consistent configurations. The rapid fall of β is found when $B_0 \sim 0.5$T and this agrees well with experimental results in CHS[8]. This shows that the β limit mechanism due to the reduction of heating efficiency plays a key role in the high β experiment in CHS.

The orbital aspects of heating efficiencies for co and counter injection are examined by modeling the two types of deviation of the drift orbit; Δ_d due to axisymmetric component of B and Δ_h due to helical component of B. In weak magnetic field the heating efficiency depends strongly on the Fourier spectrum of the magnetic field, rotational transform, and the magnetic well/hill condition, all of which are easily changeable due to the finite β effects. The consistently determined reachable β value for CHS experiments could well show the orbital aspects of experiments.

In our calculation the obtained plasma β value is lower than that of experimental results. Several reasons would be considered, e. g., contribution of multi components of beam energy, assumed energy confinement time, particle loss boundary. Further investigation is necessary to make this point clear and the more detail calculations for CHS or other heliotron/torsatron devices would be discussed elsewhere.

ACKNOWLEDGEMENTS

The authors acknowledge to the members of CHS Group and Heating Group at the National Institute for Fusion science. They also thank Prof. A. Iiyoshi and Prof. T. Sato for continuous encouragement.

References

[1] STRAIT, E.J., Phys. Plasmas **1** (1994) 1415.

[2] LAZARUS, E.A., et al., Phys. Fluids B **4** (1992) 3644.

[3] CARRERAS, B.A., et al., Nucl. Fusion **28** (1988) 1613.

[4] MOTOJIMA, O., et al., Nucl. Fusion **25** (1985) 1783.

[5] HARRIS, J.H., et al., Phys. Fluids B **2** (1990) 1353.

[6] YAMADA, H., et al., in Plasma Physics and Controlled Fusion Research 1992 (Proc. 14th Int. Conf. Würzburg, 1992), Vol. 2, IAEA, Vienna (1993) 493.

[7] OKAMURA, S., in Plasma Physics and Controlled Fusion Research 1994 (Proc. 15th Int. Conf. Sebira, 1994), IAEA-CN-60/A-6-I-4.

[8] OKAMURA, S., et al., Nuclear Fusion **35** (1995) 283.

[9] NISHIMURA, K., et al., Fusion Technol. **17**, 86 (1990).

[10] FOWLER, R.H., et al., Phys. Fluids **28** (1985) 338.

[11] MURAKAMI, S., et al., to be published in Fusion Technology.

[12] SUDO, S., et al., Nucl. Fusion **30** (1990) 11.

Figure Captions

FIG. 1. Schematic picture of the drift motion of tangentially injected NBI particle in heliotron/torsatrons. (co injection case)

FIG. 2. Regions S for calculations of the heating efficiency for three cases; a) the co injection case with $2\delta_N - 2\Delta_d - \Delta_h \geq 0$, b) the co injection case $2\delta_N - 2\Delta_d - \Delta_h < 0$, and c) the counter injection case. The shaded regions show the beam deposit regions and dotted circles are the most outer confined drift surface given by Δ_d (the least distance between the dotted circle and the last closed magnetic surface is Δ_h).

FIG. 3. Heating efficiencies of tangentially injected NBI heating in the CHS as a function of the magnetic field strength, B, for configurations with different β; (a)$\beta = 0.0\%$, (b)$\beta = 0.84\%$, (c)$\beta = 1.83\%$, and (d)$\beta = 2.38\%$. (A) co injection case with $E_b = 40$keV and (B) counter injection case with $E_b = 36$keV. The density $\langle n \rangle = 0.55 \times 10^{20}\mathrm{m}^{-3}$ is assumed to evaluate δ_N.

FIG. 4. Plots of the averaged beta values, β, as a function of the magnetic field strength, B, for configurations with different β; (a)$\beta = 0.0\%$, (b)$\beta = 0.84\%$, (c)$\beta = 1.32\%$, (d)$\beta = 1.83\%$, and (e)$\beta = 2.38\%$.

FIG. 5. Plots of the averaged beta values, β, as a function of the magnetic field strength, B, using the consistent configurations with obtained β values.

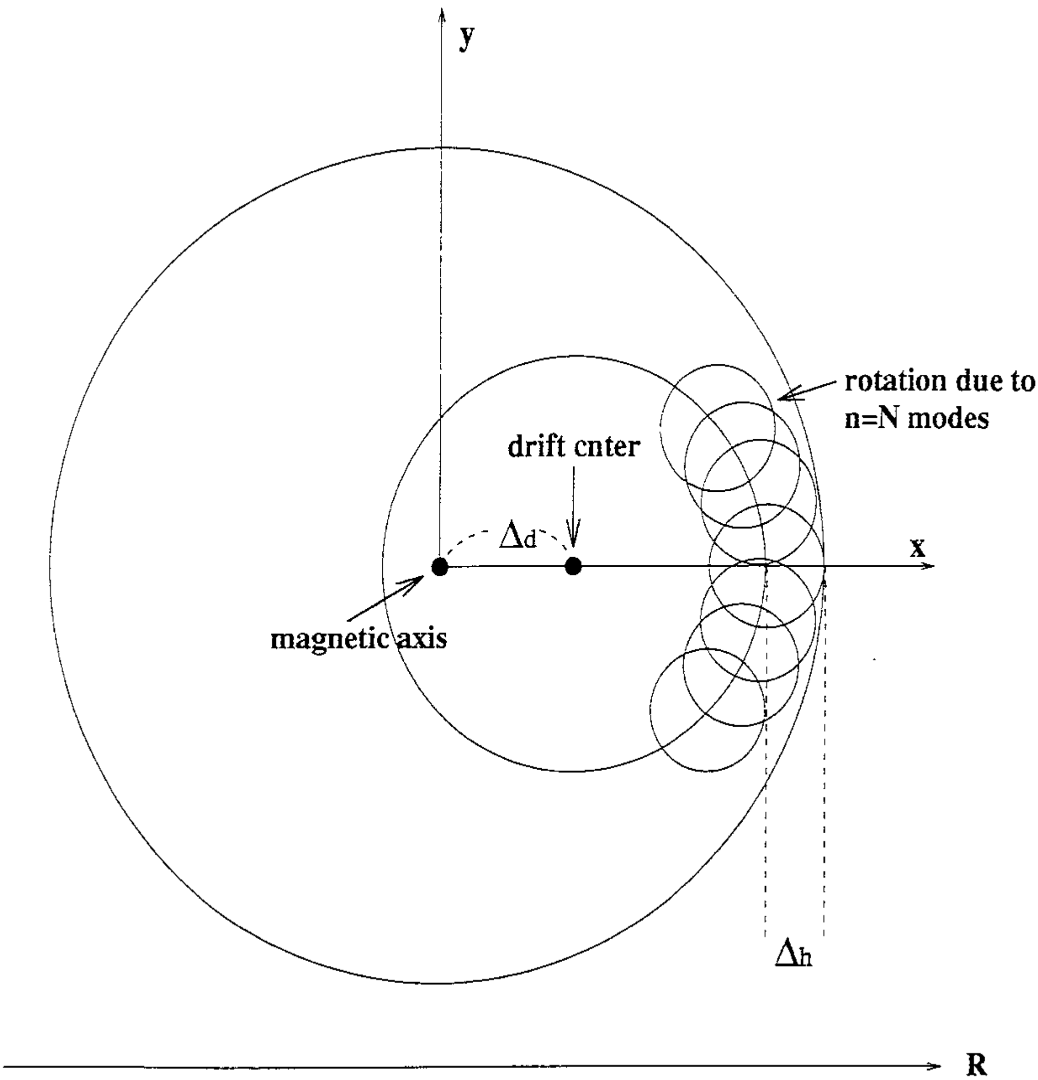
y
rotation due to
n=N modes
drift cnter
Δ_d
x
magnetic axis
Δ_h
R

FIG. 1.

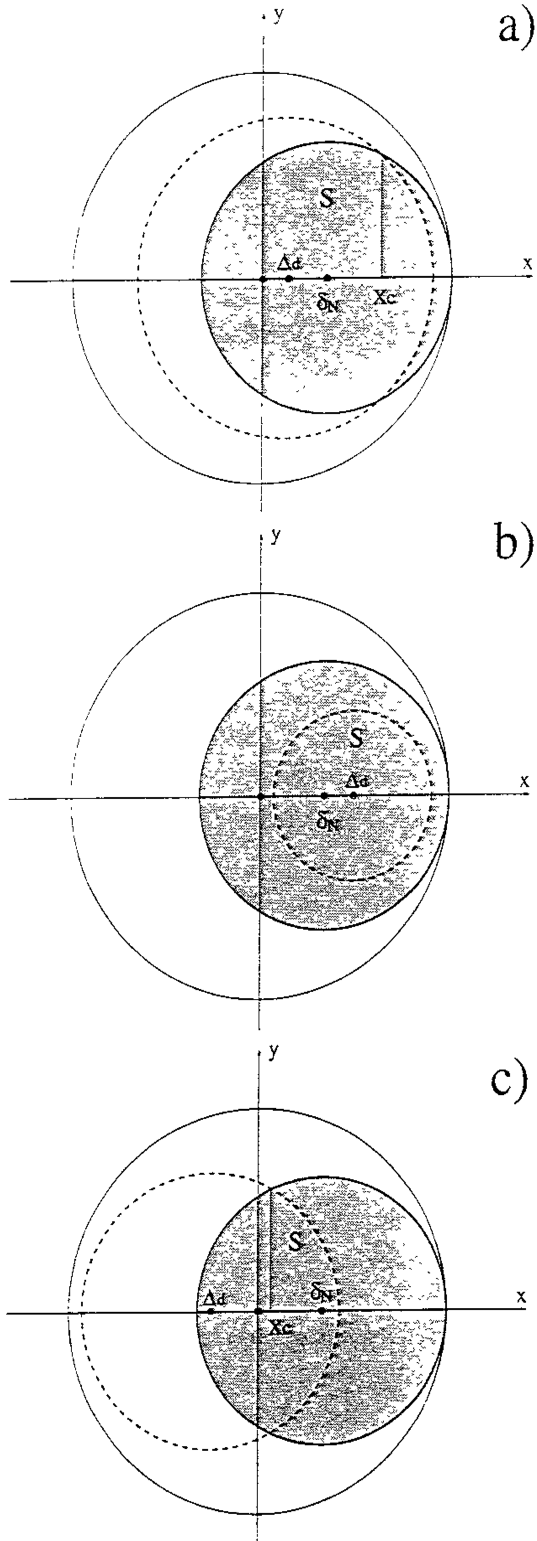

FIG. 2.

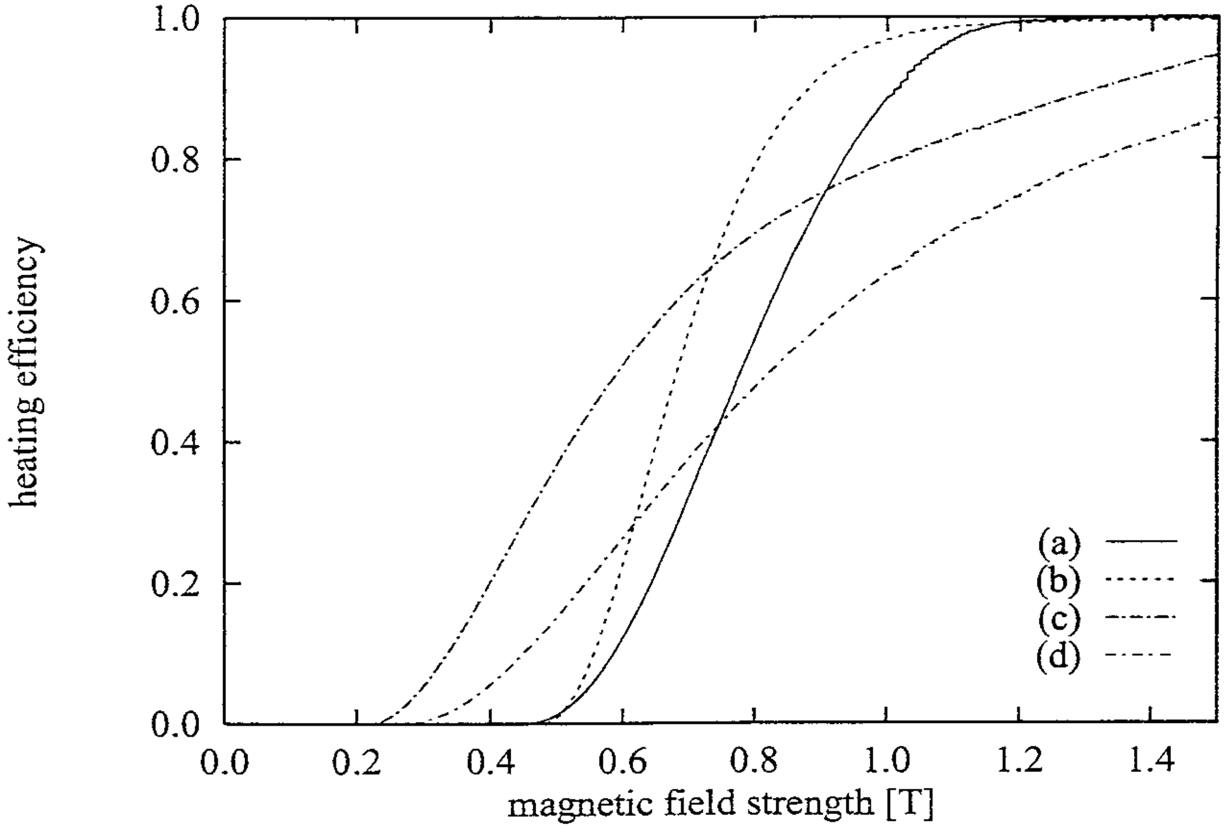
1.0
0.8
0.6
0.4
0.2
0.0
heating efficiency
0.0
0.2
0.4
0.6
0.8
1.0
1.2
1.4
magnetic field strength [T]
(a)
(b)
(c)
(d)

FIG. 3. (A)

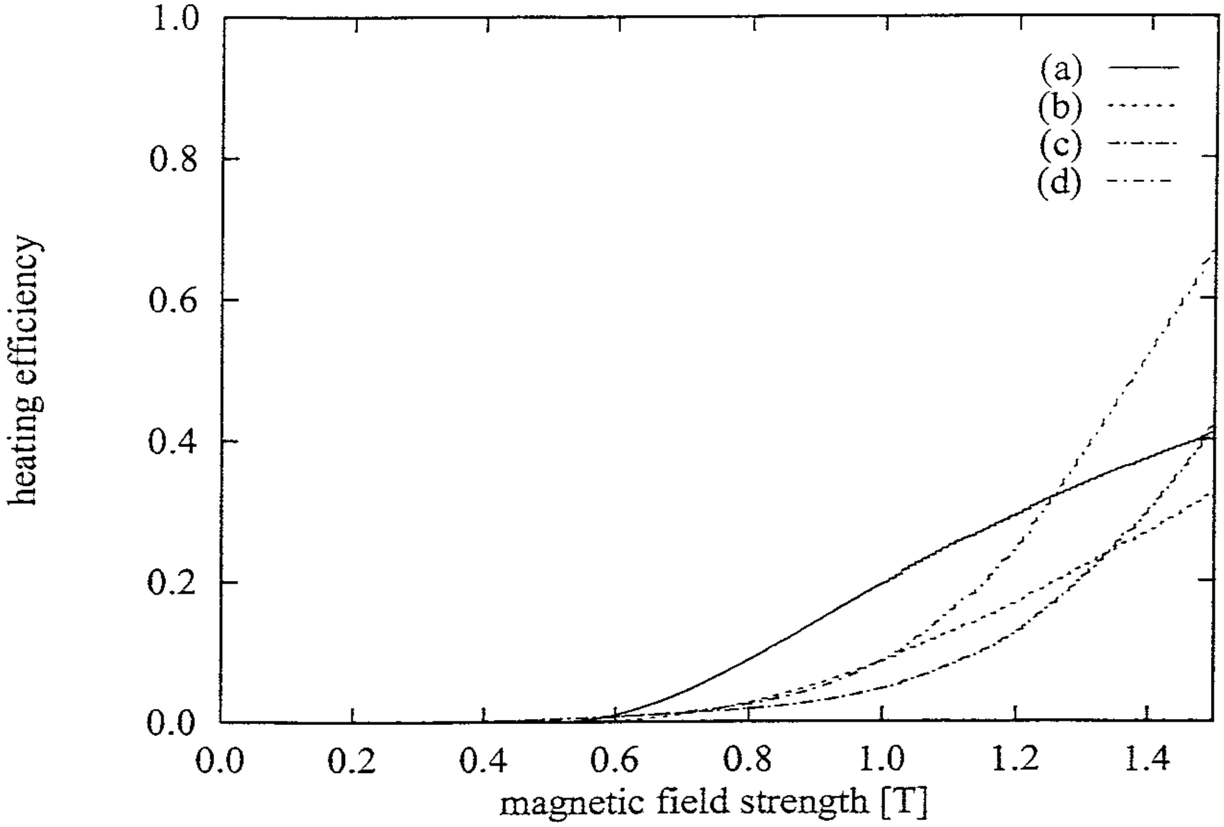

1.0
0.8
0.6
0.4
0.2
0.0
heating efficiency
(a)
(b)
(c)
(d)
0.0
0.2
0.4
0.6
0.8
1.0
1.2
1.4
magnetic field strength [T]

FIG. 3. (B)

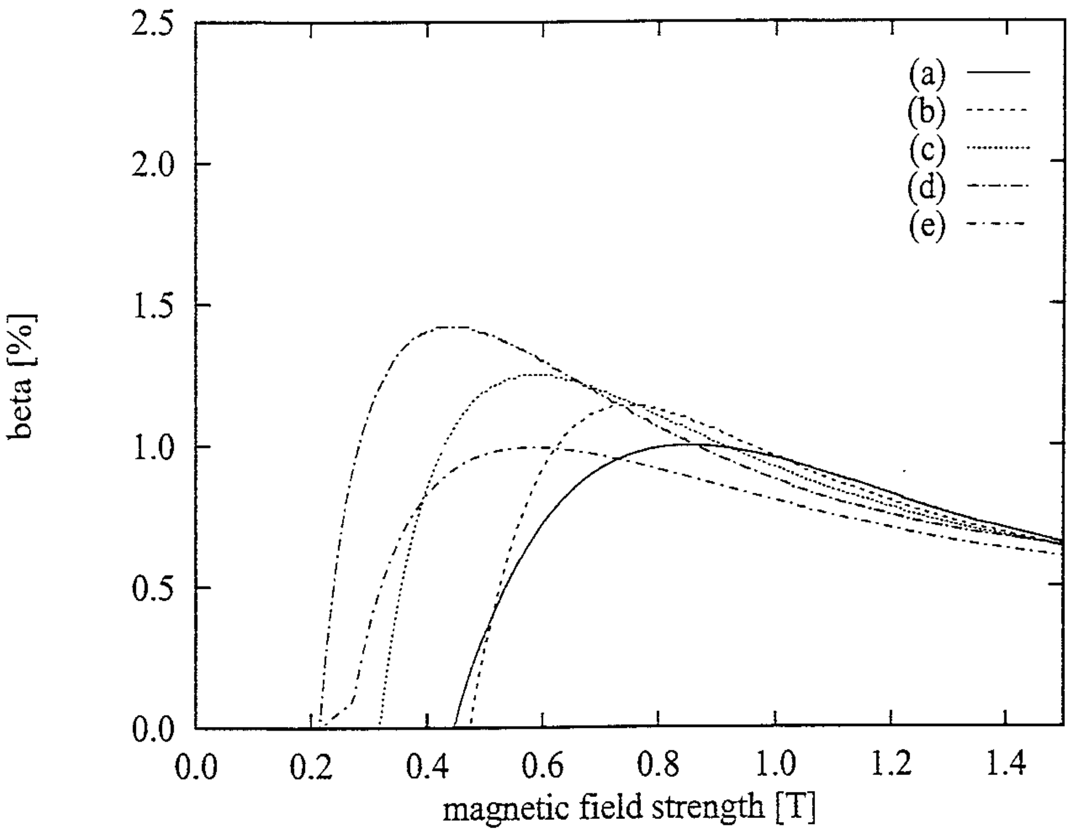

2.5
2.0
1.5
1.0
0.5
0.0
beta [%]
0.0
0.2
0.4
0.6
0.8
1.0
1.2
1.4
magnetic field strength [T]
(a)
(b)
(c)
(d)
(e)

FIG. 4.

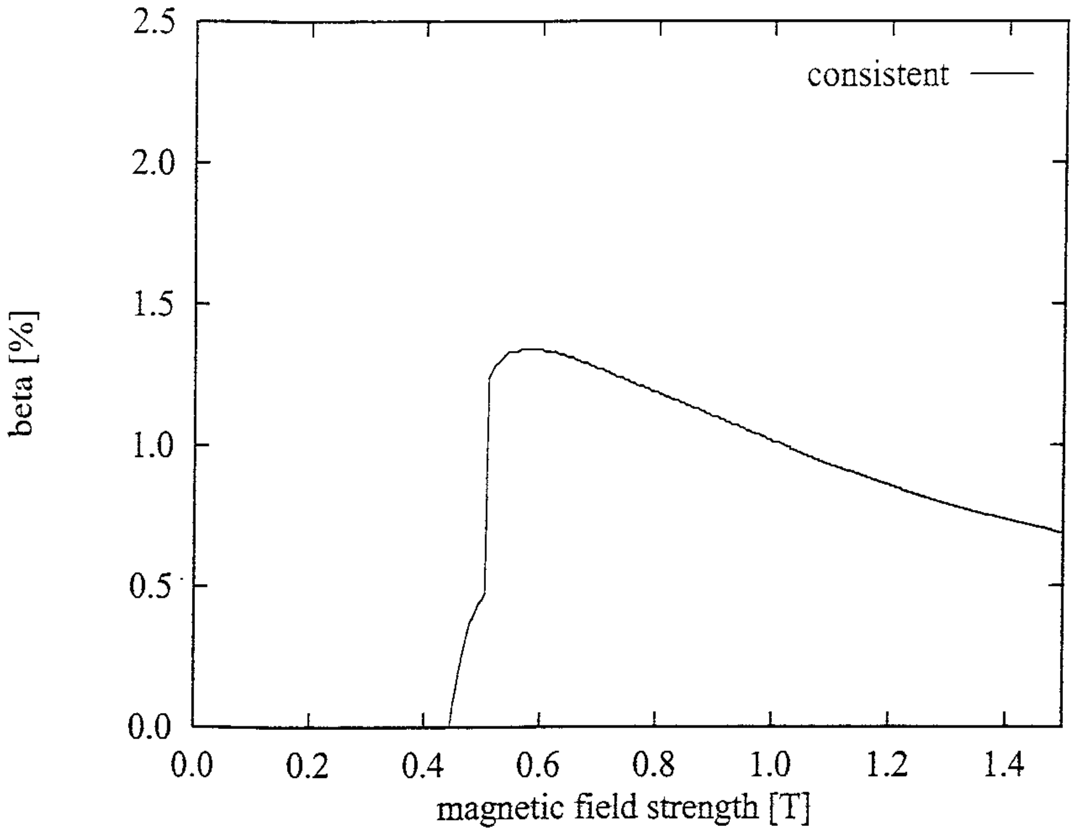
2.5
2.0
1.5
1.0
0.5
0.0
beta [%]
consistent
0.0
0.2
0.4
0.6
0.8
1.0
1.2
1.4
magnetic field strength [T]

FIG. 5.

Recent Issues of NIFS Series

NIFS-305 T. Hayashi, T. Sato, N. Nakajima, K. Ichiguchi, P. Merkel, J. Nührenberg, U. Schwenn, H. Gardner, A. Bhattacharjee and C.C.Hegna, *Behavior of Magnetic Islands in 3D MHD Equilibria of Helical Devices*; Sep. 1994 (IAEA-CN-60/D-2-II-4)

NIFS-306 S. Murakami, M. Okamoto, N. Nakajima, K.Y. Watanabe, T. Watari, T. Mutoh, R. Kumazawa and T. Seki, *Monte Carlo Simulation for ICRF Heating in Heliotron/Torsatrons*; Sep. 1994 (IAEA-CN-60/D-P-I-14)

NIFS-307 Y. Takeiri, A. Ando, O. Kaneko, Y. Oka, K. Tsumori, R. Akiyama, E. Asano, T. Kawamoto, T. Kuroda, M. Tanaka and H. Kawakami, *Development of an Intense Negative Hydrogen Ion Source with a Wide-Range of External Magnetic Filter Field*; Sep. 1994

NIFS-308 T. Hayashi, T. Sato, H.J. Gardner and J.D. Meiss, *Evolution of Magnetic Islands in a Heliac*; Sep. 1994

NIFS-309 H. Amo, T. Sato and A. Kageyama, *Intermittent Energy Bursts and Recurrent Topological Change of a Twisting Magnetic Flux Tube*; Sep.1994

NIFS-310 T. Yamagishi and H. Sanuki, *Effect of Anomalous Plasma Transport on Radial Electric Field in Torsatron/Heliotron*; Sep. 1994

NIFS-311 K. Watanabe, T. Sato and Y. Nakayama, *Current-profile Flattening and Hot Core Shift due to the Nonlinear Development of Resistive Kink Mode*; Oct. 1994

NIFS-312 M. Salimullah, B. Dasgupta, K. Watanabe and T. Sato, *Modification and Damping of Alfvén Waves in a Magnetized Dusty Plasma*; Oct. 1994

NIFS-313 K. Ida, Y. Miura, S -I. Itoh, J.V. Hofmann, A. Fukuyama, S. Hidekuma, H. Sanuki, H. Idei, H. Yamada, H. Iguchi, K. Itoh, *Physical Mechanism Determining the Radial Electric Field and its Radial Structure in a Toroidal Plasma*; Oct. 1994

NIFS-314 Shao-ping Zhu, R. Horiuchi, T. Sato and The Complexity Simulation Group, *Non-Taylor Magnetohydrodynamic Self-Organization*; Oct. 1994

NIFS-315 M. Tanaka, *Collisionless Magnetic Reconnection Associated with Coalescence of Flux Bundles*; Nov. 1994

NIFS-316 M. Tanaka,
Macro-EM Particle Simulation Method and A Study of Collisionless Magnetic Reconnection; Nov. 1994

NIFS-317 A. Fujisawa, H. Iguchi, M. Sasao and Y. Hamada,
Second Order Focusing Property of 210° Cylindrical Energy Analyzer; Nov. 1994

NIFS-318 T. Sato and Complexity Simulation Group,
Complexity in Plasma - A Grand View of Self- Organization; Nov. 1994

NIFS-319 Y. Todo, T. Sato, K. Watanabe, T.H. Watanabe and R. Horiuchi,
MHD-Vlasov Simulation of the Toroidal Alfvén Eigenmode; Nov. 1994

NIFS-320 A. Kageyama, T. Sato and The Complexity Simulation Group,
Computer Simulation of a Magnetohydrodynamic Dynamo II: Nov. 1994

NIFS-321 A. Bhattacharjee, T. Hayashi, C.C.Hegna, N. Nakajima and T. Sato,
Theory of Pressure-induced Islands and Self-healing in Three-dimensional Toroidal Magnetohydrodynamic Equilibria; Nov. 1994

NIFS-322 A. Iiyoshi, K. Yamazaki and the LHD Group,
Recent Studies of the Large Helical Device; Nov. 1994

NIFS-323 A. Iiyoshi and K. Yamazaki,
The Next Large Helical Devices; Nov. 1994

NIFS-324 V.D. Pustovitov
Quasisymmetry Equations for Conventional Stellarators; Nov. 1994

NIFS-325 A. Taniike, M. Sasao, Y. Hamada, J. Fujita, M. Wada,
The Energy Broadening Resulting from Electron Stripping Process of a Low Energy Au^- Beam; Dec. 1994

NIFS-326 I. Viniar and S. Sudo,
New Pellet Production and Acceleration Technologies for High Speed Pellet Injection System "HIPEL" in Large Helical Device; Dec. 1994

NIFS-327 Y. Hamada, A. Nishizawa, Y. Kawasumi, K. Kawahata, K. Itoh, A. Ejiri, K. Toi, K. Narihara, K. Sato, T. Seki, H. Iguchi, A. Fujisawa, K. Adachi, S. Hidekuma, S. Hirokura, K. Ida, M. Kojima, J. Koong, R. Kumazawa, H. Kuramoto, R. Liang, T. Minami, H. Sakakita, M. Sasao, K.N. Sato, T. Tsuzuki, J. Xu, I. Yamada, T. Watari,
Fast Potential Change in Sawteeth in JIPP T-IIU Tokamak Plasmas; Dec. 1994

NIFS-328 V.D. Pustovitov,
Effect of Satellite Helical Harmonics on the Stellarator Configuration; Dec. 1994

NIFS-329 K. Itoh, S-I. Itoh and A. Fukuyama,
A Model of Sawtooth Based on the Transport Catastrophe; Dec. 1994

NIFS-330 K. Nagasaki, A. Ejiri,
Launching Conditions for Electron Cyclotron Heating in a Sheared Magnetic Field; Jan. 1995

NIFS-331 T.H. Watanabe, Y. Todo, R. Horiuchi, K. Watanabe, T. Sato,
An Advanced Electrostatic Particle Simulation Algorithm for Implicit Time Integration; Jan. 1995

NIFS-332 N. Bekki and T. Karakisawa,
Bifurcations from Periodic Solution in a Simplified Model of Two-dimensional Magnetoconvection; Jan. 1995

NIFS-333 K. Itoh, S.-I. Itoh, M. Yagi, A. Fukuyama,
Theory of Anomalous Transport in Reverse Field Pinch; Jan. 1995

NIFS-334 K. Nagasaki, A. Isayama and A. Ejiri
Application of Grating Polarizer to 106.4GHz ECH System on Heliotron-E; Jan. 1995

NIFS-335 H. Takamaru, T. Sato, R. Horiuchi, K. Watanabe and Complexity Simulation Group,
A Self-Consistent Open Boundary Model for Particle Simulation in Plasmas; Feb. 1995

NIFS-336 B.B. Kadomtsev,
Quantum Telegragh : is it possible?; Feb. 1995

NIFS-337 B.B.Kadomtsev,
Ball Lightning as Self-Organization Phenomenon; Feb. 1995

NIFS-338 Y. Takeiri, A. Ando, O. Kaneko, Y. Oka, K. Tsumori, R. Akiyama, E. Asano, T. Kawamoto, M. Tanaka and T. Kuroda,
High-Energy Acceleration of an Intense Negative Ion Beam; Feb. 1995

NIFS-339 K. Toi, T. Morisaki, S. Sakakibara, S. Ohdachi, T.Minami, S. Morita, H. Yamada, K. Tanaka, K. Ida, S. Okamura, A. Ejiri, H. Iguchi, K. Nishimura, K. Matsuoka, A. Ando, J. Xu, I. Yamada, K. Narihara, R. Akiyama, H. Idei, S. Kubo, T. Ozaki, C. Takahashi, K. Tsumori,
H-Mode Study in CHS; Feb. 1995

NIFS-340 T. Okada and H. Tazawa,
Filamentation Instability in a Light Ion Beam-plasma System with External Magnetic Field; Feb. 1995

NIFS-341 T. Watanbe, G. Gnudi,

A New Algorithm for Differential-Algebraic Equations Based on HIDM; Feb. 13, 1995

NIFS-342 Y. Nejoh,
New Stationary Solutions of the Nonlinear Drift Wave Equation; Feb. 1995

NIFS-343 A. Ejiri, S. Sakakibara and K. Kawahata,
Signal Based Mixing Analysis for the Magnetohydrodynamic Mode Reconstruction from Homodyne Microwave Reflectometry; Mar.. 1995

NIFS-344 B.B.Kadomtsev, K. Itoh, S.-I. Itoh
Fast Change in Core Transport after L-H Transition; Mar. 1995

NIFS-345 W.X. Wang, M. Okamoto, N. Nakajima and S. Murakami,
An Accurate Nonlinear Monte Carlo Collision Operator; Mar. 1995

NIFS-346 S. Sasaki, S. Takamura, S. Masuzaki, S. Watanabe, T. Kato, K. Kadota,
Helium I Line Intensity Ratios in a Plasma for the Diagnostics of Fusion Edge Plasmas; Mar. 1995

NIFS-347 M. Osakabe,
Measurement of Neutron Energy on D-T Fusion Plasma Experiments; Apr. 1995

NIFS-348 M. Sita Janaki, M.R. Gupta and Brahmananda Dasgupta,
Adiabatic Electron Acceleration in a Cnoidal Wave; Apr. 1995

NIFS-349 J. Xu, K. Ida and J. Fujita,
A Note for Pitch Angle Measurement of Magnetic Field in a Toroidal Plasma Using Motional Stark Effect; Apr. 1995

NIFS-350 J. Uramoto,
Characteristics for Metal Plate Penetration of a Low Energy Negative Muonlike or Pionlike Particle Beam: Apr. 1995

NIFS-351 J. Uramoto,
An Estimation of Life Time for A Low Energy Negative Pionlike Particle Beam: Apr. 1995

NIFS-352 A. Taniike,
Energy Loss Mechanism of a Gold Ion Beam on a Tandem Acceleration System: May 1995

NIFS-353 A. Nishizawa, Y. Hamada, Y. Kawasumi and H. Iguchi,
Increase of Lifetime of Thallium Zeolite Ion Source for Single-Ended Accelerator: May 1995